Onset of DNA Aggregation in Presence of Monovalent and Multivalent Counterions

Yoram Burak, Gil Ariel, and David Andelman
School of Physics and Astronomy, Raymond and Beverly Sackler Faculty of Exact Sciences, Tel Aviv University, Tel Aviv 69978, Israel

ABSTRACT We address theoretically aggregation of DNA segments by multivalent polyamines such as spermine and spermidine. In experiments, the aggregation occurs above a certain threshold concentration of multivalent ions. We demonstrate that the dependence of this threshold on the concentration of DNA has a simple form. When the DNA concentration c_{DNA} is smaller than the monovalent salt concentration, the threshold multivalent ion concentration depends linearly on c_{DNA}, having the form $\alpha c_{DNA} + \beta$. The coefficients α and β are related to the density profile of multivalent counterions around isolated DNA chains, at the onset of their aggregation. This analysis agrees extremely well with recent detailed measurements on DNA aggregation in the presence of spermine. From the fit to the experimental data, the number of condensed multivalent counterions per DNA chain can be deduced. A few other conclusions can then be reached: 1), the number of condensed spermine ions at the onset of aggregation decreases with the addition of monovalent salt; 2), the Poisson-Boltzmann theory overestimates the number of condensed multivalent ions at high monovalent salt concentrations; and 3), our analysis of the data indicates that the DNA charge is not overcompensated by spermine at the onset of aggregation.

INTRODUCTION

Condensation and aggregation of DNA, induced by multivalent counterions, have been extensively studied in the past two decades (for a review, see Bloomfield et al., 2000, and references therein). The term condensation usually refers to the collapse of a single, long DNA chain. Condensation plays an important role in storage and packing of DNA; for example, in viral capsids (Gelbart et al., 2000). Aggregation of DNA is a closely related phenomenon, where multiple chains attract each other and form a variety of condensed mesophases of complex structure (Pelta et al., 1996a,b). In both phenomena multivalent counterions play a crucial role, screening the electrostatic repulsion between charged strands of DNA and mediating an effective attraction.

A variety of tri- and tetravalent ions can induce aggregation and condensation, among them the polyamines spermidine (3^+) and spermine (4^+) (Chattoraj et al., 1978; Gosule and Schellman, 1978; Tabor and Tabor, 1984), as well as cobalt-hexamine (Widom and Baldwin, 1980, 1983). In typical experiments on aggregation (Pelta et al., 1996b; Raspaud et al., 1998; Saminathan et al., 1999) multivalent ions are gradually added to a solution with fixed concentration of DNA segments and monovalent salt. Two such examples for spermine and spermidine are reproduced in Fig. 1 (Pelta et al., 1996b). As the multivalent ion concentration is raised above a certain threshold, DNA segments begin to aggregate, and precipitate from the solution. Above the aggregation threshold, the DNA concentration decreases gradually or abruptly, depending on various parameters such as the monovalent salt concentration and total DNA concentration. Further addition of multivalent ions at higher concentrations reverses the aggregation. Above a second, redissolution threshold, all the DNA is redissolved in the solution (Fig. 1). The redissolution threshold (above which all the DNA redissolves) is almost independent on the DNA concentration. Its value can be attributed to screening of electrostatic interactions by multivalent ions (Raspaud et al., 1998).

The aggregation threshold, where the onset of aggregation occurs, is the main experimental phenomenon addressed in our theoretical article. The multivalent ion concentration at the onset depends strongly on the monovalent salt and DNA concentrations. This dependence has been recently measured in detail for short (150 basepair) DNA segments in presence of spermine (Raspaud et al., 1998), and is reproduced in Fig. 2. The figure shows measurements of spermine concentrations at the onset of aggregation, for DNA concentrations ranging over four orders of magnitude and for four different monovalent salt concentrations: 2, 13, 23, and 88 mM. At very low DNA concentration, the spermine concentration depends strongly on the monovalent salt concentration. At higher DNA concentration it has only a weak dependence on the monovalent ion concentration but the spermine concentration is proportional to the DNA concentration, indicating that a certain number of spermine counterions are required, per DNA base, to induce aggregation. The solid line in Fig. 2, adapted from Raspaud et al. (1998), corresponds to a ratio: $c_{z,aggr}/c_{DNA} = 0.20$, where $c_{z,aggr}$ is the spermine concentration at the aggregation onset and c_{DNA} is the DNA concentration. This linear relation fits a large number of the experimental points in the intermediate DNA concentration range. It has been suggested by Raspaud et al. (1998, 1999) that the deviations from this line, at low and high DNA concentrations, represent two distinct physical regimes that need to be analyzed separately from the intermediate regime, where the linear fit works well.

Submitted March 30, 2003, and accepted for publication May 28, 2003.

Address reprint requests to David Andelman, School of Physics and Astronomy, Tel Aviv University, Tel Aviv, Israel 69978. Tel.: 972-3-640-7239; Fax: 972-3-642-2979; E-mail: andelman@post.tau.ac.il.

0006-3495/03/10/2100/11 $2.00

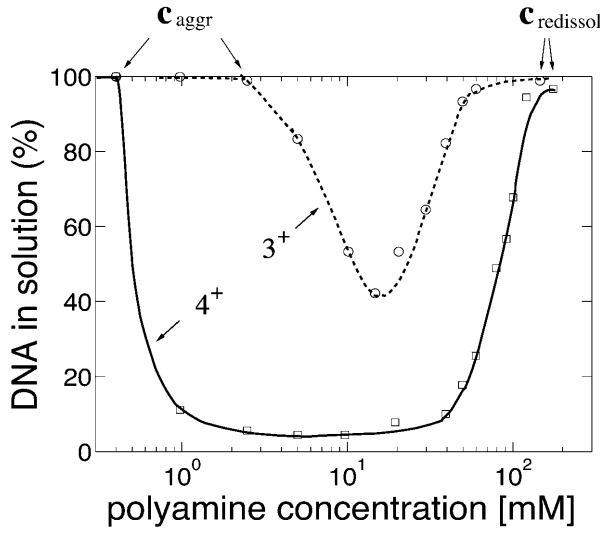

FIGURE 1 Percent of solubilized DNA, as function of polyamine concentration. Squares, spermine; circles, spermidine. Solid and dashed lines are guides for the eye. DNA and NaCl concentrations are 3 mM and 25 mM, respectively. Below the aggregation threshold, c_{aggr}, and above the redissolution threshold, $c_{redissol}$, all the DNA is dissolved. The data is adapted from Pelta et al. (1996b).

In this work we focus on the onset of aggregation, and specifically on its dependence on the DNA concentration. We show that this dependence is simple for all the range of DNA concentration. Furthermore, for c_{DNA} smaller than the monovalent salt concentration we show that this dependence is linear: $c_{z,aggr} = \alpha c_{DNA} + \beta$. The coefficient β is the multivalent counterion concentration far away from the DNA chains, whereas α accounts for the excess of multivalent ions around each chain. These quantities can be extracted, e.g., from the four experimental curves of Fig. 2.

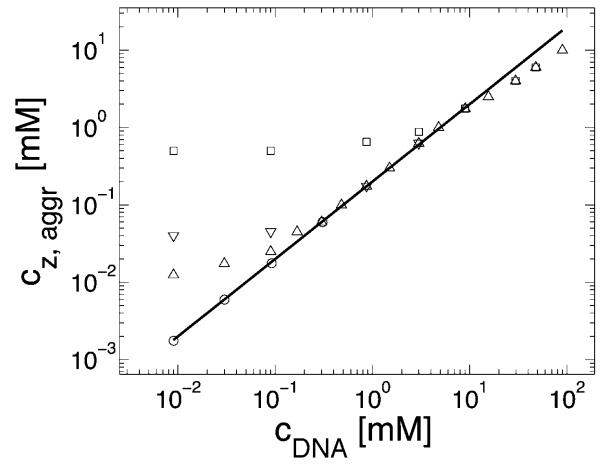

FIGURE 2 Spermine concentration, $c_{z,aggr}$, at the onset aggregation, as a function of DNA monomer concentration c_{DNA}. Data is shown for four monovalent salt concentrations: 2 mM (○); 13 mM (Δ); 23 mM (∇); and 88 mM (□). Solid line corresponds to the fixed ratio of $c_{z,aggr}/c_{DNA} = 0.20$. The data is adapted from Raspaud et al. (1998).

Several further conclusions are then drawn on the onset of DNA aggregation and on the counterion distribution around each double-stranded DNA.

THEORETICAL CONSIDERATIONS

Consider an aqueous solution containing monovalent (1:1) salt, multivalent (z:1) salt, and DNA segments below their threshold for aggregation. Throughout this article, the DNA solution is assumed to be dilute enough such that the DNA segments do not overlap. We also assume that these DNA segments can be regarded as rigid rods. The concentrations of added monovalent salt, multivalent salt, and DNA monomers are denoted by c_s, c_z, and c_{DNA}, respectively. These are the solute concentrations per unit volume as controlled and adjusted in experiments. We will assume that the monovalent and multivalent salts have the same type of co-ion, so that altogether there are three ion species in the solution:

1. A multivalent counterion contributed from the z:1 multivalent salt, of concentration c_z.
2. A monovalent counterion contributed by monovalent salt of concentration c_s, and by counterions dissociated from the DNA, of concentration c_{DNA}: in total $c_{DNA} + c_s$.
3. Co-ions coming from both z:1 and 1:1 salts, of concentration $c_s + zc_z$.

Each DNA segment attracts a layer of oppositely charged counterions referred to as the condensed counterions. As long as the typical distance between segments is large compared to the electrostatic screening length κ^{-1}, the electrostatic potential decays exponentially to zero far away from the DNA segments. In turn, the concentrations of the three ion species decay to well-defined *bulk* values denoted by c_1^∞ for the monovalent ions and c_z^∞ for those that are z-valent. These concentrations should be distinguished from the concentrations c_s and c_z introduced above, which are the average concentrations of added salts regulated experimentally.

The Debye screening length, κ^{-1}, characterizing the exponential decay of the electrostatic potential, is determined by the bulk concentrations of all three ionic species:

$$\kappa^2 = 4\pi l_B \left[c_1^\infty + z^2 c_z^\infty + \left(c_1^\infty + z c_z^\infty\right)\right], \qquad (1)$$

where the third term is the co-ion concentration. It is equal to $c_1^\infty + z c_z^\infty$ due to charge neutrality far from the DNA where the potential decays to zero. The above equation makes use of the Bjerrum length, $l_B = e^2/(\varepsilon k_B T)$, equal to ~7 Å in aqueous solution at room temperature. $k_B T$ is the thermal energy, e is the electron charge, and $\varepsilon = 80$ is the dielectric constant of water. The Debye length as well as c_z^∞ are shown schematically in Fig. 3. Other quantities that will be defined below are also indicated in this figure.

In dilute solutions different DNA segments do not overlap. Following previous works, we introduce a cell model,

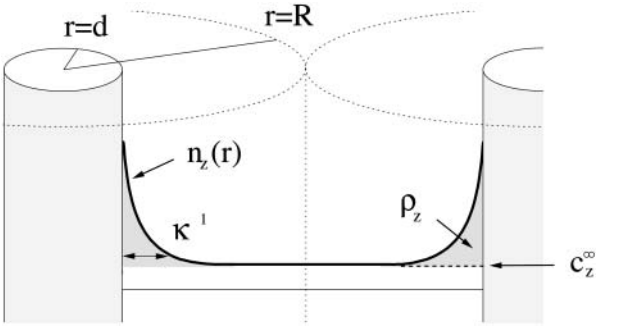

FIGURE 3 Schematic representation of the multivalent density profile, $n_z(r)$, between two neighboring DNA segments, each modeled as a cylinder of radius d. Here r is the distance from the axis of the left DNA strand. The radius $r = R$ corresponds to the interstrand mid-distance and is the unit cell radius. The density decays to its bulk value c_z^∞ on distances larger than κ^{-1}, where κ^{-1} is the Debye length defined in Eq. 1. The excess density of multivalent ions, ρ_z, is indicated by the shaded areas.

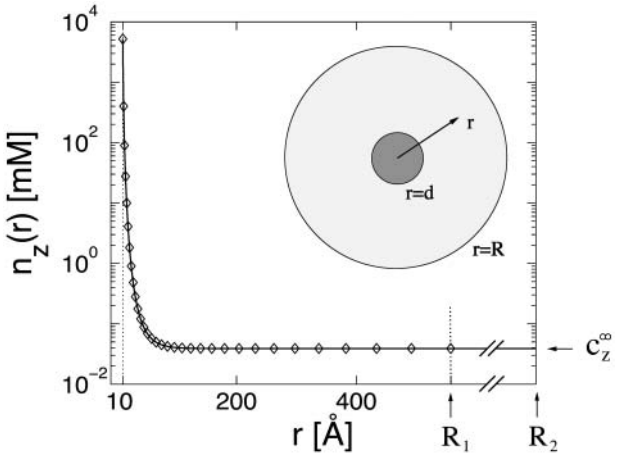

FIGURE 4 Density profile $n_z(r)$ of 4-valent ions as function of r, the distance from the DNA axis, on a semilog plot, calculated using the Poisson-Boltzmann equation in a cell model, where the DNA segment is modeled as a uniformly charged cylinder. The cell model is shown schematically in the *inset*. Two cell sizes are shown, with outer radii $R_1 = 560$ Å ($c_{DNA} = 1$ mM) and $R_2 = 1.8 \times 10^4$ Å ($c_{DNA} = 10^{-3}$ mM), indicated by arrows. In both cases, the radius of closest approach of ions to the charged chain is at $r = d$, where $d = 10$ Å, as indicated by a dotted vertical line. The boundary condition at the inner cylinder matches the linear charge density of DNA ($1e$/1.7 Å). The bulk densities of monovalent and multivalent ions, c_1^∞ and c_z^∞, are chosen to be the same in the two cells, leading to practically identical density profiles. The solid line represents the larger cell (R_2), and diamonds are used for the smaller cell (R_1). Density profiles of monovalent counterions and co-ions are not shown but are also practically identical in the two cells. Average salt concentrations are $c_s = 22$ mM and $c_z = 0.21$ mM in the smaller cell, and $c_s = 23$ mM, $c_z = 0.039$ mM in the larger cell. Bulk concentrations are $c_1^\infty = 23$ mM and $c_z^\infty = 0.039$ mM. Note that these bulk concentrations are practically identical to the salt concentrations in the larger cell. Note also that $c_1^\infty > c_s$ in the smaller cell, reflecting the contribution of the counterions released by the DNA.

also shown schematically in Fig. 3. Note that the model serves to illustrate the subsequent derivations but is not essential for the validity of our main results. In the cell model, each segment, of a cylindrical cross-section, is at the center of a cylindrical cell of radius R and area $A = \pi R^2$ such that

$$c_{DNA} = 1/(aA). \tag{2}$$

Namely, each DNA monomer occupies a specific volume aA, where $a \simeq 1.7$ Å is the average charge separation on the chain taken hereafter as the monomer length.

We will assume below that the DNA solution is dilute enough so that R is large compared to the Debye length κ^{-1}. This assumption is essential for our derivation and can be verified for all the experimental data considered in this article. Density profiles of the three ion species are then practically identical to those near an isolated DNA segment with the same bulk concentrations c_1^∞, c_z^∞. In other words, the profiles are determined uniquely by c_1^∞ and c_z^∞, with practically no dependence (or, more precisely, an exponentially small dependence) on the DNA monomer concentration. A demonstration of this claim is presented in Fig. 4, using the Poisson-Boltzmann theory in a cell model. For two very different values of R corresponding to different c_{DNA}, the counterion profiles match perfectly when the values of c_1^∞ and c_z^∞ are the same. Note that the average concentrations of added salts, c_s and c_z, have different values in the two cells because of the contribution of condensed ions.

The total number of z-valent counterions, per cell unit length, is given by:

$$Ac_z = Ac_z^\infty + \rho_z(c_1^\infty, c_z^\infty), \tag{3}$$

where ρ_z is the excess number of z-valent ions per unit length near the DNA. Throughout the article we use the symbol c to denote concentrations per unit volume and ρ for concentrations per DNA unit length. The excess ρ_z can be evaluated in the limit of infinite cell radius, corresponding to an isolated chain,

$$\rho_z = 2\pi \int_0^\infty r\,dr[n_z(r) - c_z^\infty], \tag{4}$$

where $n_z(r)$ is the z-valent local counterion concentration at distance r from the axis of symmetry, and $n_z(\infty) = c_z^\infty$. Following the discussion in the previous paragraph, the excess ρ_z is determined uniquely by c_1^∞ and c_z^∞. Its exact functional dependence on these variables is generally not known, although it can be evaluated approximately, e.g., using the Poisson-Boltzmann equation or in computer simulations.

For monovalent counterions we have, in a similar fashion,

$$Ac_s + Ac_{DNA} = Ac_1^\infty + \rho_1(c_1^\infty, c_z^\infty), \tag{5}$$

where ρ_1, the excess of monovalent counterions per unit length, is defined as in Eq. 4, and $Ac_{DNA} = 1/a$ is the DNA charge density per unit length. The extra term in the left-hand side of Eq. 5 originates from monovalent counterions contributed by the DNA monomers. Using Eq. 2 we can rewrite Eqs. 3 and 5 as

$$c_z = c_z^\infty + a\rho_z(c_1^\infty, c_z^\infty)c_{DNA}, \quad (6)$$

and

$$c_s = c_1^\infty + [a\rho_1(c_1^\infty, c_z^\infty) - 1]c_{DNA}. \quad (7)$$

These two equations relate the experimentally adjustable c_s, c_z, and c_{DNA} to the bulk densities c_1^∞ and c_z^∞, that, in turn, are important because they determine the ion density profiles.

In the limit of infinite DNA dilution, $c_{DNA} = 0$, and therefore $c_z = c_z^\infty$ and $c_s = c_1^\infty$. At any finite DNA concentration, c_z and c_s are not equal to c_z^∞ and c_1^∞, respectively, because each segment captures some of the multivalent ions and releases a number of monovalent ones. Equations 6 and 7 express the correction to c_s, c_z at given c_1^∞, c_z^∞ for both mono- and multivalent counterion species. The dimensionless quantities $a\rho_1$, $a\rho_z$ are the excess of the mono- and multivalent counterion species, respectively, per DNA monomer.

We would like to emphasize the generality of Eqs. 6 and 7. They do not depend on the assumption of parallel DNA residing in the middle of oriented cylindrical unit cells, or on any mean-field approximation for the distribution of counterions. The only assumption required to derive Eqs. 6 and 7 is that the average distance between DNA segments is large compared with the Debye length. Although Eqs. 6 and 7 are correct for any c_s, c_z, and c_{DNA} below the onset of DNA aggregation, we will be interested below specifically in the aggregation onset.

Onset of aggregation

Our aim now is to find how the value of c_z at the onset of aggregation, $c_{z,aggr}$, depends on c_{DNA}. We will assume that this aggregation onset depends on c_1^∞ and c_z^∞, but not on the average distance between DNA chains. We motivate this assumption by the fact that c_1^∞ and c_z^∞ determine the density profile of multivalent counterions around the DNA chains, which, in turn, mediate the attraction necessary for aggregation. Before discussing this assumption in more detail, let us first consider its consequences. We can imagine an experiment where c_z^∞ is gradually increased while c_1^∞ is kept fixed. Aggregation will start, in this experiment, above a certain threshold value of c_z^∞. Our assumption is that this threshold does not depend on c_{DNA}. In real experiments, however, c_z is adjusted rather than c_z^∞, and c_s is kept fixed rather than c_1^∞. To find the threshold value in terms of the experimentally available c_z, we need to map c_1^∞, c_z^∞ onto c_s, c_z. This mapping is described by Eqs. 6–7, and involves c_{DNA}. It is only through this mapping that c_{DNA} will affect the threshold of aggregation.

The limit of $c_{DNA} \ll c_s$

The limit $c_{DNA} \ll c_s$ offers a particularly simple dependence of $c_{z,aggr}$ on c_{DNA} and is considered first. Most models and experiments indicate that monovalent counterions cannot overcharge DNA segments. Hence the monovalent excess, $a\rho_1$, in Eq. 7, is a number between zero and one, because the excess monovalent charge is smaller than that of DNA. From Eq. 7, $|c_s - c_1^\infty| \ll c_s$ as long as $c_{DNA} \ll c_s$. It is then possible to replace c_1^∞ by c_s, leading to a simplification of Eq. 6:

$$c_z = c_z^\infty + a\rho_z(c_s, c_z^\infty)c_{DNA}. \quad (8)$$

Note that c_{DNA} is indeed smaller than c_z in most of the experimental points in Fig. 2. However a similar simplification cannot be applied for c_s because it is typically much smaller than c_s, and often smaller than c_{DNA}.

According to our principal assumption, aggregation starts at a threshold value $c_z^\infty = c_z^*$, which does not depend on c_{DNA} (whereas $c_{z,aggr}$, the average multivalent salt concentration, does depend on c_{DNA} through Eq. 8). Similarly, the density profile at the threshold does not depend on c_{DNA}, because it is determined by $c_1^\infty = c_s$ and c_z^*. The excess of z-valent counterions, as determined from this profile, is equal to:

$$\rho_z^* = \rho_z(c_s, c_z^*), \quad (9)$$

with no dependence on c_{DNA}. Using the threshold values c_z^* and ρ_z^* in Eq. 8, we find that the average concentration of z-valent ions at the onset of aggregation is

$$c_{z,aggr}(c_{DNA}) = c_z^* + a\rho_z^* c_{DNA}. \quad (10)$$

This is the threshold concentration that was measured experimentally in Raspaud et al. (1998). Note that, in Eq. 10, c_z^* as well as ρ_z^* depend on the monovalent salt concentration, c_s, but the explicit dependence is omitted for clarity.

The simple relationship expressed by Eq. 10 is one of our main results. As a visualization of this result we refer again to Fig. 3. The quantities ρ_z, c_z^∞, and the density profile $n_z(r)$ are indicated in this figure. At the onset of aggregation, c_z^∞ is equal to c_z^* and does not depend on c_{DNA} (or equivalently, on the spacing between DNA segments, R). As c_{DNA} is increased the distance between DNA strands decreases. The onset values of c_z^∞ and ρ_z do not change, but the contribution of ρ_z to the average concentration increases, leading to an increase in $c_{z,aggr}$.

The coefficients $a\rho_z^*$ and c_z^* of the linear dependence in Eq. 10 are the coefficients α and β defined in the introduction section. They can be easily found from the experimental data: c_z^* is the value of $c_{z,aggr}$ in the limit of infinite DNA dilution, $c_{DNA} \to 0$, since in this limit $c_z = c_z^\infty = c_z^*$. The excess at the onset, ρ_z^*, can be found from the slope of $c_{z,aggr}$ as function of c_{DNA}. Before presenting a detailed comparison with experiments, we generalize the treatment for small c_{DNA} to arbitrary values.

The case of $c_{DNA} \geq c_s$

When c_{DNA} is of the same order as c_s or larger, corrections to c_1^∞ must be taken into account, as expressed by Eq. 7, and the linear relation of Eq. 10 no longer holds. The ion density profiles as well as c_s and c_z are now determined by the two

variables c_1^∞ and c_z^∞. The relation between c_1^∞ and c_z^∞ and the experimentally controlled c_s, c_z, and c_{DNA} is given by Eqs. 6–7. In terms of c_1^∞, c_z^∞ the criterion for aggregation remains the same as in the previous case:

$$c_z^\infty = c_z^*(c_1^\infty). \tag{11}$$

Equations 6, 7, and 11, with the three unknowns c_1^∞, c_z^∞, and c_z, lead to a unique solution for $c_{z,aggr}$. Note that c_1^∞ is larger than c_s because of counterions coming from the DNA as can be seen in Eq. 7, where $a\rho_1 - 1$ is negative. In Eq. 10, c_s is replaced by c_1^∞, which is larger than c_s for large c_{DNA}. Hence, increasing c_{DNA} has an effect similar to addition of monovalent salt. As noted above, this effect is significant only for $c_{DNA} > c_s$.

COMPARISON WITH EXPERIMENT

Raspaud et al. (1998) measured the spermine (z=4) concentration c_z at the onset of aggregation as a function of c_{DNA} for four values of c_s and with c_{DNA} ranging over four orders of magnitude—from 10^{-2} to 10^2 mM. We fitted the data (E. Raspaud and J.-L. Sikorav, private communication) for each c_s to a straight line according to Eq. 10. The least square fit presented in Fig. 5 takes into account the experimental error bars and data points up to $c_{DNA} = 10$ mM. In Fig. 5 *a* the fit is shown using a linear scale which covers the range of c_{DNA} only up to $c_{DNA} = 1.5$ mM for clarity purposes. Due to the large range of c_{DNA} it is impossible to show all the data on the linear scale of Fig. 5 *a*. Instead, the same data and linear lines are shown in Fig. 5 *b* on a log-log scale over the full experimental range of c_{DNA}.

The linear fit is very good for all four values of monovalent salt concentration c_s. Note that for $c_s = 88$ mM the fit is very good up to the largest value of $c_{DNA} = 48$ mM reported in the experiment, although our fit takes into account only data points up to $c_{DNA} = 10$ mM. It was previously suggested (Raspaud et al., 1998) that a separate regime exists for $c_{DNA} \gtrsim 10$ mM, characterized by a power law relation between c_z and c_{DNA} with an exponent smaller than unity. Our analysis suggests a different conclusion. The fit clearly demonstrates that the relation is linear all the way up to $c_{DNA} = 48$ mM, as predicted by Eq. 10. Note also that even at $c_{DNA} = 48$ mM we have $c_{DNA} < c_s$, so the assumptions leading to Eq. 10 are still valid.

The only points in Fig. 5 *b* that deviate significantly from the fit are the three points where $c_s = 13$ mM (*triangles*) and $c_{DNA} > 20$ mM (two of these points coincide with points having $c_s = 88$ mM, shown using *square symbols*.) This deviation is easily explained by the fact that $c_{DNA} \gg c_s$ so that corrections to c_1^∞ must be taken into account. For example, at $c_{DNA} = 90$ mM the nominal monovalent counterion concentration is 103 mM, taking into account counterions contributed by the DNA. To find $c_1{}^\infty$ we need to subtract the condensed counterions, as determined by ρ_1. We can estimate ρ_1 at this point by solving the Poisson-Boltzmann equation in a unit cell with the appropriate radius. The chemical potentials of the three ion species are tuned such that their concentrations match the known values of c_z and c_s. This leads to an estimate: $c_1^\infty \simeq 68$ mM. Hence, c_z at the onset of aggregation should lie a little below the continuation of the $c_s = 88$ mM line which is, indeed, where it is found. The trend for $c_s = 13$ mM can probably be seen already at the point $c_{DNA} = 15$ mM, although the deviation at this point is still within the range of experimental error. The few other experimental points with $c_{DNA} \approx c_s$ deviate slightly from the straight line as well (still within experi-

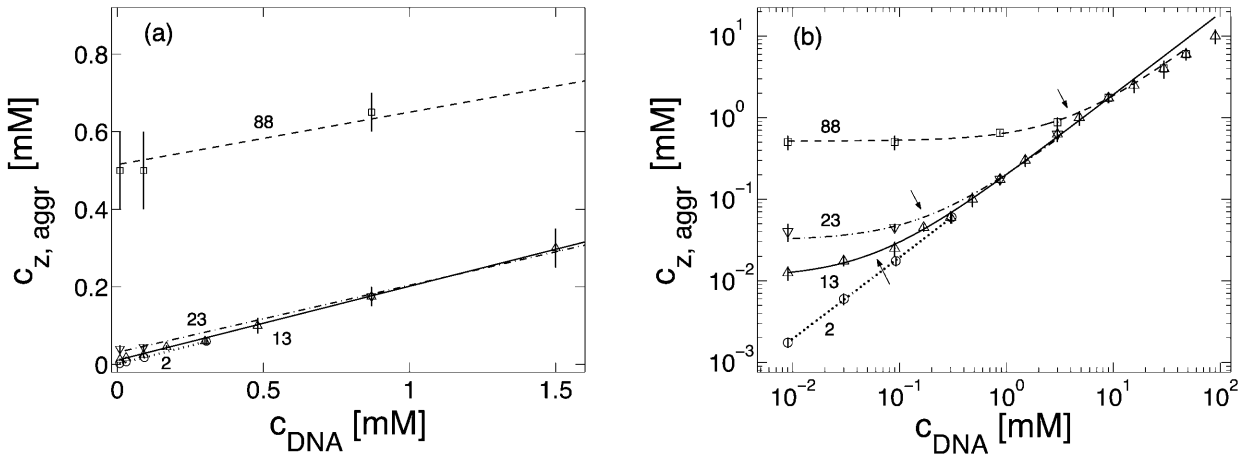

FIGURE 5 Spermine concentration at the onset of aggregation $c_{z,aggr}$ as a function of c_{DNA}, fitted to the form derived in Eq. 10 (different line types are used for different salt concentrations). Value of c_s (in mM) is indicated next to each curve. Experimental data is adapted from Raspaud et al. (1998) and shown in the following symbols: $c_s = 2$ mM (○); 13 mM (Δ); 23 mM (∇); and 88 mM (□). Experimental error bars (E. Raspaud, private communication) are indicated by vertical lines. The fitted lines and experimental points are shown using a linear scale in *a*, up to $c_{DNA} = 1.5$ mM, and a log-log scale in *b*, up to $c_{DNA} = 100$ mM, allowing all data points to be shown on the same plot. Only the data up to $c_{DNA} = 10$ mM was used for the linear fit. The crossover values of c_{DNA}, as defined by Eq. 14, are indicated by arrows in *b*.

mental error bars). In all these cases the deviation is in the direction corresponding to a higher value of c_s, as expected.

A linear relation of the form $c_{z,aggr} = \alpha c_{DNA} + \beta$, was previously suggested on empirical basis for aggregation induced by spermidine (3^+), on a smaller range of DNA concentrations (Osland and Kleppe, 1977; Pelta et al., 1996b). Although this result looks similar to our prediction on the onset of aggregation, it is not directly related to our analysis because $c_{z,aggr}$ was taken in those works to be the transition midpoint. This is the point where half of the maximal precipitation of DNA is reached. Our analysis does not apply at the transition midpoint since it requires all the DNA segments to be well separated from each other. Indeed, the coefficient α, related to the transition midpoint, was found in Osland and Kleppe (1977) and Pelta et al. (1996b) to be of order 10^2, much larger than unity. Such a value of α cannot be interpreted as the excess of spermidine ions per monomer near isolated chains.

The parameters of the linear fit in Fig. 5 are summarized in Table 1 for the four experimentally used values of c_s.

Crossover in the log-log plot

For presentation purposes we plot in Fig. 5 *b*, $c_{z,aggr}$ vs. c_{DNA} on a log-log scale, as appeared in Raspaud et al. (1998). The linear relation that was found between these two quantities is not clearly manifested on the log-log plot, because a linear dependence of the form $y = \alpha x + \beta$ is not easily recognized in such a plot. Furthermore, such a linear relation appears on a log-log plot to be *artificially* characterized by two distinct behaviors, at low and high values of the independent variable. These two behaviors were mentioned in Raspaud et al. (1998) and can be seen in Fig. 5 *b*. However, they do not represent in our opinion two real physical regimes and can be understood by taking the logarithm of Eq. 10. For small c_{DNA} (large R),

$$\log c_{z,aggr} \simeq \log c_z^*. \tag{12}$$

That is, c_z does not depend on c_{DNA} as is seen in Fig. 5 *b* in the small c_{DNA} limit. In the opposite limit of large c_{DNA} (small R):

$$\log c_{z,aggr} \simeq \log c_{DNA} + \log a\rho_z^*. \tag{13}$$

Here, the linear dependence of $c_{z,aggr}$ on c_{DNA} yields a line of slope 1 in the same figure.

The crossover between these apparent behaviors occurs when the number of bulk and excess ions are the same:

TABLE 1 Fit parameters used in Fig. 5

c_s [mM]	c_z* [mM]	$a\rho_z$*
2	0 ± 0.0003	0.194 ± 0.020
13	0.011 ± 0.002	0.191 ± 0.013
23	0.031 ± 0.005	0.173 ± 0.025
88	0.52 ± 0.05	0.135 ± 0.026

$$c_{DNA} = \frac{c_z^*}{a\rho_z^*}. \tag{14}$$

When c_{DNA} is much smaller than this crossover value, the number of excess multivalent ions near DNA segments is negligible compared to their total number. In the other extreme of c_{DNA} much larger than the crossover value, the number of free multivalent ions is negligible compared to the excess ions, and nearly all multivalent ions are bound to the DNA.

For the experimental data in Fig. 5 the crossover value is equal to 0.06, 0.18, and 3.9 mM for c_s =13, 23, and 88 mM, respectively, and smaller than 1.5×10^{-3} mM for c_s = 2 mM. The first three crossover points are indicated by arrows in Fig. 5 *b*.

DNA AGGREGATION AND COUNTERION CONDENSATION

We separate the discussion following our results in three parts. The first addresses the conditions required for DNA aggregation. The coefficients of the linear relation in Eq. 10, c_z* and ρ_z*, have a definite physical meaning. Their values, as extracted from the experimental data, provide insight on these conditions. The second part deals with condensation of counterions on DNA (to be distinguished from condensation of DNA chains). The general relation $\rho_z = \rho_z(c_1^\infty, c_z^\infty)$ that was introduced in Eqs. 3–4 is a property of counterion condensation on isolated chains. By extracting the values of ρ_z, c_1^∞, and c_z^∞ at the onset of DNA aggregation, we can learn about exact density profiles of spermine around DNA, and compare our findings with approximations such as Poisson-Boltzmann theory. Finally, we comment on our main assumption, which was used in the theoretical considerations section.

Conditions at the onset of aggregation

Most of the proposed theoretical models for interchain attraction and aggregation (see, for example, Arenzon et al., 1999; Borukhov et al., 2001, 2002; Ha and Liu, 1997; Nguyen et al., 2000; Olvera de la Cruz et al., 1995; Raspaud et al., 1998; Wittmer et al., 1995) regard the charged chain as surrounded by a layer of condensed ions which is usually modeled as a one-dimensional gas. This layer mediates an interchain attraction, and the models predict the number of condensed ions required to initiate aggregation of the chains. In the current work we do not address this theoretical problem, but rather concentrate on what can be inferred from the experimental results using the analysis presented in the previous section. This analysis provides insight on the conditions prevailing at the onset of aggregation. In particular, the excess ρ_z* characterizes the number of condensed multivalent counterions that are present near each chain at the onset. Although, in general, the notion of condensed

counterions is somewhat ill-defined as it depends on which ions are regarded as bound to the DNA, we show in the Appendix that in our case it does have a reasonably well-defined meaning. Furthermore, the number of condensed multivalent ions per monomer is practically the same as $a\rho_z^*$.

The excess of multivalent counterions per monomer, $a\rho_z^*$, is shown in Fig. 6 as a function of c_s. All values are taken from Table 1, as extracted from the experimental data. The dashed line is a linear fit. Two different axis scales are used on the left and right of the plot. The left axis shows the value of $a\rho_z^*$. The right one shows the part of DNA charge that is compensated by condensed multivalent ions, $za\rho_z^*$, where $z = 4$ for spermine. From the plot we deduce the following two conclusions:

1. The number of condensed multivalent ions (per DNA monomer) $a\rho_z^*$ at the onset decreases as the monovalent salt concentration increases, with variation between 0.19 and 0.14. A possible reason for this trend may be that the bare electrostatic repulsion between chains is decreased due to increased screening. Hence a smaller number of multivalent ions is required to overcome this repulsion. The change in ρ_z^* may also be related to the competition between monovalent and multivalent ions in the aggregated DNA state.
2. The data indicates that there is no over-charging of the DNA by spermine at the onset (see also Nguyen et al., 2000) since $za\rho_z^* < 1$. At higher concentration of spermine, beyond the threshold, we do not rule out the possibility of DNA overcharging, as was suggested by Nguyen et al. (2000).

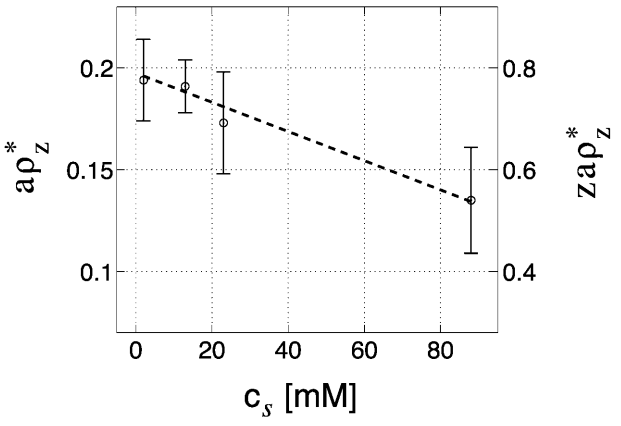

FIGURE 6 Excess of multivalent counterions per monomer at the onset of aggregation, $a\rho_z^*$, as function of c_s. All values are taken from Table 1, as extracted from the experimental data of Raspaud et al. (1998). Error bars are indicated by vertical bars and the dashed line is a linear fit to be used as a guide to the eye. On the right axis, $za\rho_z^*$ is shown, where $z = 4$ for spermine. This value is equal to the fraction of DNA charge compensated by the condensed multivalent ions. Note that, according to the Manning condensation theory, the same quantity is equal to 0.94, for tetravalent ions and no added salt.

Although ρ_z^* decreases with increase of c_s, it is of the same order of magnitude for all the c_s values in Table 1. In contrast, c_z^* varies in Table 1 over more than three orders of magnitude. As was previously suggested (Olvera de la Cruz et al., 1995; Raspaud et al., 1998), this large variation in c_z^* is a result of competition between monovalent and multivalent counterions. We discuss the relation between ρ_z^* and c_z^* to some extent in the following subsection. A more detailed analysis of this relation, emphasizing the role of competition between the two counterion species, will be presented in a separate publication (see also Belloni et al., 1984; Wilson and Bloomfield, 1979; Wilson et al., 1980).

Counterion condensation

We now turn to analyze the condensation of monovalent and multivalent ions around DNA. Each line in Table 1 provides a measurement of the excess ρ_z at certain values of c_1^∞ and c_z^∞. The general relation $\rho_z(c_1^\infty, c_z^\infty)$ is a property of counterion density profiles around isolated DNA segments. Hence, the data in Table 1 can be used to test any particular theory used to calculate such ion distributions.

The most simple model to consider is the Poisson-Boltzmann (PB) theory (see Andelman, 1994; Guéron and Weisbuch, 1980; Le Bret and Zimm, 1984; Oosawa, 1971). In Table 2 we compare the excess predicted by PB theory with the experimental result, by solving the PB equation such that c_1^∞ and c_z^∞ match the experimental values of c_s and c_z^* from Table 1. The excess is then calculated from the PB density profile, and compared with the experimental value of $a\rho_z$ (equal to $a\rho_z^*$ of Table 1). The DNA is modeled as a uniformly charged cylinder of radius $d = 10$ Å.

Inspection of the results in Table 2 shows that there is a reasonable agreement with experiment (within the error bars) for the three smaller values of $c_s = 2$, 13, and 23 mM. However, for $c_s = 88$ mM there is a 30% deviation. The two data points with $c_{DNA} > 10$ mM that were not taken into account in the linear fit of Fig. 5 suggest that ρ_z is closer to the lower bound of the experimental error range, whereas the PB value is larger than the upper bound.

Overall, the agreement with PB theory (Table 2) is surprisingly good, considering that PB theory does not work so well for bulky multivalent ions. Deviations from PB theory have several sources. One of these sources is specific molecular details such as the geometrical shape of ions, DNA structure, and short-range interactions. Another source

TABLE 2 Excess of 4-valent ions near DNA compared with PB theory

c_1^∞ [mM]	c_z^∞ [mM]	$a\rho_z$ (exp)	$a\rho_z$ (PB)
2	0 ± 0.0003	0.194 ± 0.020	0.186 ± 0.005
13	0.011 ± 0.002	0.191 ± 0.013	0.178 ± 0.002
23	0.031 ± 0.005	0.173 ± 0.025	0.172 ± 0.002
88	0.52 ± 0.05	0.135 ± 0.026	0.164 ± 0.002

for deviations are ion-ion correlations between spermine molecules, computed in theories which go beyond the mean-field approximation. However, these correlations tend to increase the number of bound multivalent counterions (Lyubartsev and Nordenskiöld, 1997), whereas for $c_s = 88$ mM, the number of bound multivalent counterions is decreased. We conclude that correlation effects by themselves are not the main source of the deviations seen in Table 2. In addition the data analysis does not indicate overcharging of the DNA. Such an effect may be expected if correlation effects are strong (Nguyen et al., 2000).

In Fig. 7 we compare the DNA aggregation data with PB predictions at finite DNA concentrations. For each DNA concentration the PB equation is solved in a cylindrical cell of the appropriate radius. The multivalent counterion concentration c_z is gradually increased until the onset is reached, and its onset value, $c_{z,aggr}$, is plotted as function of c_{DNA}. Two different criteria are used to determine the onset $c_{z,aggr}$. In Fig. 7 *a* it is chosen as the point where c_z^∞ is equal to the experimental value c_z* of Table 1, whereas in Fig. 7 *b*, the onset is chosen as the point where $\rho_z = \rho_z$*. To span all the data range we use, for convenience, a log-log plot, as in Fig. 5 *b*.

On a linear scale, all the lines in Fig. 7, *a* and *b*, are straight lines. This fact serves as additional confirmation of our general analysis in the Theoretical Considerations section. In accordance with our analysis, both c_z* and ρ_z are constant along each line, and the slope of each line is equal to $a\rho_z$. Note that the relation between c_z* and ρ_z is determined in Fig. 7 within the PB approximation, while in Fig. 5 both of these coefficients are related to the actual counterion density profiles in the experimental system. The use of the PB equation is the source of deviations from experimental data in Fig. 7.

On first inspection the match with experiment in Fig. 7 *a* is very good, whereas the match in Fig. 7 *b* is not as good. On closer inspection it is seen that the fit in Fig. 7 *b* is not good for small values of c_{DNA}, while it is actually better than in Fig. 7 *a* for large c_{DNA}. With the PB equation it is not possible to obtain a perfect fit for both small and large c_{DNA} because the values of c_z^∞ and ρ_z are not independent. Fixing $c_z^\infty = c_z$* (as in Fig. 7 *a*) sets a value of ρ_z that is different from ρ_z*, and the opposite happens in Fig. 7 *b*. The fit in Fig. 7 *a* is quite good even for large c_{DNA} because the values of ρ_z* are of similar order of magnitude for all four lines.

Deviations as in Fig. 7 are inevitable if any approximations are used to model the distribution of counterions around DNA. Note, however, that within such approximate models our general theoretical considerations should apply, as long as the total number of ions in the system is counted properly. Such a model that goes beyond PB was proposed in Nguyen and Shklovskii (2001). Indeed, within this model a linear relationship similar to Eq. 10 was found.

The experimental results analyzed in this section may be influenced, to a certain degree, by the fact that there was more than one type of monovalent counterion in the system. For the three higher salt concentrations, except for $c_s = 2$ mM, the solution contained 10 mM of Tris–H^+ ions in addition to Na^+ (Raspaud et al., 1998). For the largest salt concentration, 88 mM, where significant deviations from PB theory are found, this effect is probably negligible. Another detail regarding the TE buffer is that the Tris ions may be only partly ionized. If only 80% of Tris is ionized, as suggested in Tang et al. (1997), the concentrations $c_s = 13$

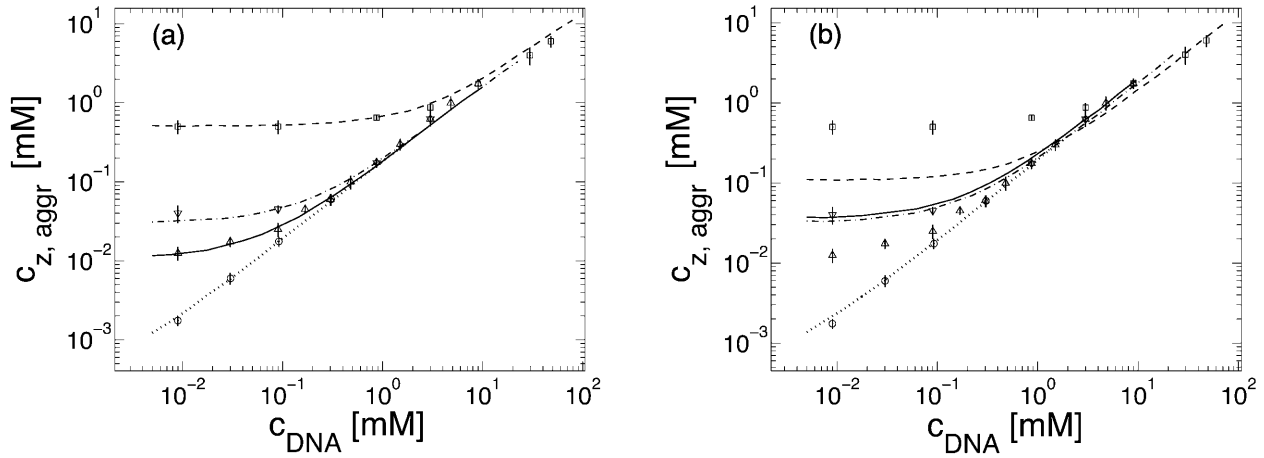

FIGURE 7 Spermine concentration (in mM) as a function of DNA monomer concentration (mM) at the onset of aggregation, calculated using the PB equation. Two different criteria are used in *a* and *b* to determine the onset: in *a*, c_z^∞, as calculated using the PB equation, is equal to the experimental value of c_z* from Table 1. In *b*, ρ_z of PB theory is equal to ρ_z* from Table 1. The radius of DNA is taken as $d = 10$ Å. Log-log plot is used to show the five decades of DNA concentrations. For each c_s the plot covers experimental data up to $c_{DNA} = c_s$. For larger c_{DNA}, corrections due to changes in c_1^∞ should be taken into account, as was discussed in the preceding section. All notations are the same as in Fig. 5.

mM, 23 mM, and 88 mM should be reduced by 2 mM. Although this will have only a small effect on our results, it will improve both the comparison with PB and the fit with the dashed line in Fig. 6, for the point $c_s = 13$ mM. For the two other concentrations of 23 mM and 88 mM the effect will be negligible.

Further comments on underlying model assumption

Our underlying assumption, that the onset of aggregation depends uniquely on c_1^∞ and c_z^∞ (but not on c_{DNA}), is an approximation that can be justified on several different levels but deserves further and more thorough investigation. The most simple motivation for this assumption is that multivalent ions, in the vicinity of the chains, mediate the attraction necessary for aggregation. In turn, the number of condensed multivalent ions near each chain is determined by c_1^∞ and c_z^∞.

Let us first suppose that aggregation starts when a net attraction appears between two chains. This assumption may be justified if chains are sufficiently long and their translational entropy can be neglected. To find the onset of two-chain attraction the free energy of a two-chain complex should be calculated as a function of the distance between the two chains. This free energy represents the effective interaction between the two chains, mediated by the ionic solution. The counterion distribution near each chain will not be the same for close-by and for isolated chains. However, in both cases, the concentrations must decay to their bulk values throughout the solution, c_1^∞ and c_z^∞. This requirement serves as a boundary condition, imposed at a large distance from the two chains. It will determine uniquely the counterion distribution between the chains, as well as the free energy associated with the two-chain complex. Hence c_1^∞ and c_z^∞ determine the effective interaction between chains, and in particular whether an attraction occurs at a certain range of interchain separations; in terms of these variables the onset of two-chain attraction does not depend on c_{DNA}.

Strictly speaking, the onset of aggregation and the onset of two-chain attraction are not the same. The aggregate phase involves interactions between multiple chains, whereas chains in the dilute phase interact very weakly with each other. Aggregation starts when the free energy per chain is equal in the dilute and aggregate phases. Note that the chemical potential of each ion species must be the same in the two phases, and that in the dilute phase these chemical potentials are directly related to c_1^∞ and c_z^∞. Hence c_1^∞ and c_z^∞ determine the free energy per chain in the two phases. The approximation of independence on c_{DNA} neglects the translational entropy of DNA segments, which can be justified for long enough and rigid segments. It also neglects contributions from interactions between chains in the dilute phase, which are assumed to be small compared to the free energy of the single DNA-counterion complexes.

SUMMARY

We have shown that the onset of aggregation at finite (nonzero) DNA concentration, $c_{z,aggr}$, is determined by the onset in the limit of infinite DNA dilution. For DNA monomer concentration smaller than that of monovalent salt, $c_{DNA} \lesssim c_s$, the multivalent counterion concentration at the onset, $c_{z,aggr}$, depends linearly on c_{DNA}. The coefficients of this linear dependence are the bulk concentration of multivalent counterions and their excess relative to the bulk near each DNA segment. Both of these coefficients are of theoretical interest and can be extracted from the available experimental data.

Our main assumption is that the onset of aggregation can be related to the ion density profiles around each chain. Hence, it is uniquely determined by c_1^∞ and c_z^∞, the bulk concentrations of the two counterion species, respectively. Our results and fit to experiment strongly support this assumption. Nevertheless, we believe that more detailed theoretical and experimental investigations are needed to fully understand its range of validity. For example, it will be of interest to test experimentally the equilibration of a DNA solution through a dialysis membrane, with a cell containing only counterions (Braunlin et al., 1982; Plum and Bloomfield, 1988; Subirana and Vives, 1981). This procedure allows a direct control of the ionic bulk concentrations.

To predict precisely the onset of aggregation, the structure of the aggregated phase must be considered. Nevertheless, it is instructive to focus only on single chains at the onset, as is often done. At the aggregation onset the electrostatic repulsion between isolated chains in solution must be overcome by a sufficiently strong attraction mediated by multivalent counterions. This number of counterions is expected to depend only weakly on physical parameters such as the monovalent salt concentration. Our analysis does not address directly the question of the onset origin, but merely supports the fact that the number of condensed multivalent ions at the onset, $a\rho_z^*$, is of the same order of magnitude, regardless of the c_s value. A more refined result of our analysis is that $a\rho_z^*$ is not constant but decreases with increase of c_s. On the other hand, c_z^*, the value of c_z^∞ at the onset, depends strongly on c_s. This is mainly a result of the competition between monovalent and multivalent ions, as will be addressed in a separate publication.

Our analysis also sheds light on counterion condensation on DNA, which is independent on the criterion for DNA aggregation. The experimental data indicates that for high c_s the number of spermine ions in the vicinity of DNA is smaller than the prediction of Poisson-Boltzmann theory. A similar trend was observed in computer simulations (Lyubartsev and Nordenskiöld, 1997) of spermidine (3^+) and NaCl in contact with DNA. Spermidine binding was affected by addition of monovalent salt more strongly than the Poisson-Boltzmann prediction. For high salt concentrations spermidine binding was considerably smaller. In the

computer simulations both molecular-specific interactions, the geometrical shape of the constituents and interion correlations were taken into account. All these effects, and in particular the geometry of the spermidine molecule, which is similar to that of spermine, were found to play an important role.

The above analysis demonstrates that specific interactions play an important role in determining the threshold of aggregation. In the dilute phase these interactions strongly influence the competition between monovalent and multivalent ions and the free energy of DNA-counterion complexes. Similarly, specific interactions play a prominent role in the dense phase (Strey et al., 1998). Force measurements under osmotic stress (Rau et al., 1984; Rau and Parsegian, 1992a,b) provide a wealth of information on these interactions.

In conclusion, the physical parameters extracted here from experiment on the onset of DNA aggregation provide insight on the conditions required for aggregation, and on condensation of ions around DNA. These parameters may turn out to be of great value in assessment of various theoretical models. Additional detailed experiments may further deepen our understanding of these complex phenomena.

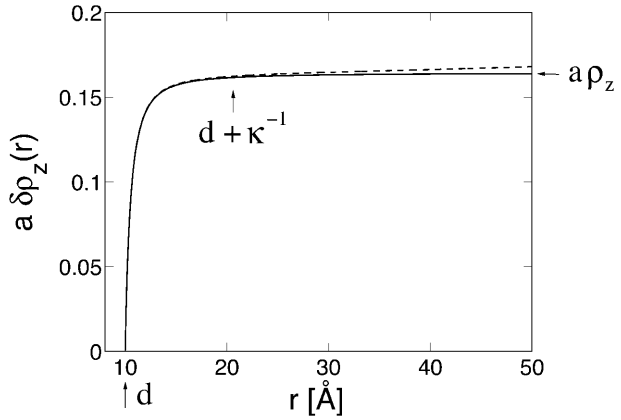

FIGURE 8 Excess of 4-valent ions per DNA monomer, up to a distance r from the axis of a charged cylinder of radius $d = 10$ Å (modeling the DNA) as obtained using the Poisson-Boltzmann equation (*solid line*). The excess $\delta\rho_z(r)$ is defined in Eq. A1. The number of charges per unit length on the cylinder is $1/a$ where $a = 1.7$ Å to fit DNA values. The bulk densities of monovalent and multivalent ions are $c_1^\infty = 88$ mM, $c_z^\infty = 0.52$ mM, yielding $\kappa^{-1} = 10.0$ Å. The quantity $\delta\rho_z$ (*solid line*) can be compared with the total number of 4-valent ions (*dashed line*) up to a distance r from the cylinder. The distance $d + \kappa^{-1}$ from the DNA axis is indicated by a vertical arrow, and characterizes the decay of the density profile far away from the DNA.

APPENDIX

In this Appendix we discuss the relation between the excess and the number of condensed ions. The latter quantity is not as well-defined as the former, but relates more naturally to the aggregation mechanism. The notion of condensed ions suggests that some ions are bound to the charged chain whereas others are free. In reality there is a density profile that extends all the way from $r = d$ to $r = R$ with no definite separation between condensed and free ions. In the following we define condensed ions rather loosely as the number of ions up to a certain characteristic distance from the chain (Belloni et al., 1984; Wilson et al., 1980). We show that for multivalent ions this number does not depend strongly on the choice of this characteristic distance. Hence, the number of condensed ions is reasonably well defined. Moreover, the excess number of multivalent counterions, which can be directly calculated from the experimental data, is nearly identical to this quantity. This point will be further explained below.

Fig. 8 shows the excess of 4-valent counterions $\delta\rho_z(r)$ up to a distance r from the DNA axis, as a function of r:

$$\delta\rho_z(r) = 2\pi \int_0^r r'\,dr'[n_z(r') - c_z^\infty], \tag{A1}$$

with the limit $\delta\rho_z(\infty) = \rho_z$ of Eq. 4. The density profile was calculated using the Poisson-Boltzmann equation, with the radius of DNA taken as $d = 10$ Å and with bulk densities of ions as in the last line of Table 1: $c_s = c_1^\infty = 88$ mM, and $c_z^\infty = 0.52$ mM.

Three observations can be made. First, most, but not all, of the excess z-valent ions are localized very close to the DNA, at a distance of order λ/z, where λ is the Gouy-Chapman length (see Andelman, 1994):

$$\lambda = \frac{1}{2\pi l_B \sigma} = \frac{d}{l_B \rho_{DNA}}, \tag{A2}$$

where σ is the average charge per unit area on the cylinder surface, $\sigma = \rho_{DNA}/2\pi d$, and $\rho_{DNA} = 1/a$ is the DNA charge per unit length. At room temperature the Bjerrum length $l_B \simeq 7$ Å, and for DNA with 4-valent counterions $\lambda/z \simeq 0.6$ Å. Second, the counterions within a layer of a few times the Debye length ($\kappa^{-1} = 10.0$ Å in Fig. 8) neutralize the DNA charge. Nearly all the excess distribution is in this layer. Third, to estimate the total amount of counterions in the condensed layer of thickness $\alpha\kappa^{-1}$, where α is a number of order unity, we need to add $\delta\rho_z$ to the bulk contribution, $\pi\alpha^2\kappa^{-2}c_z^\infty$. Using κ from Eq. 1, the latter is equal to:

$$\left(\frac{\alpha^2}{4l_B}\right)\frac{c_z^\infty}{2c_1^\infty + z(z+1)c_z^\infty}. \tag{A3}$$

In experiment, c_z^∞ is much smaller than c_1^∞ at the onset, and the bulk contribution of Eq. A3 can be neglected relative to ρ_z, for α of order unity. This can be seen specifically in Fig. 8 by comparing the solid and dashed lines.

The outcome of the above discussion is that ρ_z, defined in Eq. 4 as the excess of counterions throughout the cell, can be regarded, to a good approximation, as the total number of counterions within a condensation layer whose thickness is approximately the Debye length. For typical concentration ranges as considered here we do not expect that this outcome will change, even for models going beyond Poisson-Boltzmann theory.

As a further demonstration, the number of multivalent counterions up to several different distances from the DNA is shown in Table 3, as calculated in a unit cell using the Poisson-Boltzmann equation. For each c_s in Table 1 we find the Poisson-Boltzmann density profile such that $c_1^\infty = c_s$ and

TABLE 3 Number of z-valent counterions, per DNA monomer, up to several different distances from the DNA axis, compared with $a\rho_z$

c_s [mM]	d + 10 Å	d + 20 Å	$d + \kappa^{-1}$	$d + 2\kappa^{-1}$	$a\rho_z$
2	0.191	0.193	0.194	0.194	0.194
13	0.187	0.190	0.190	0.191	0.191
23	0.171	0.172	0.172	0.173	0.173
88	0.134	0.135	0.134	0.135	0.135

$\rho_z = \rho_z^*$, and then calculate the number of multivalent ions (per DNA monomer) up to the following distances from the DNA radius: 10 Å, 20 Å, κ^{-1}, and $2\kappa^{-1}$. The values of κ^{-1}, as obtained from Eq. 1 are equal to 68, 26, 20, and 10 Å for $c_s = 2$, 13, 23, and 88 mM, respectively. These numbers are compared with $a\rho_z^*$. All the different measures in Table 3 yield results that are very close to each other.

We are grateful to E. Raspaud and J.-L. Sikorav for numerous discussions and for providing us with their unpublished experimental data. We also wish to thank I. Borukhov, H. Diamant, M. Kozlov, A. Lyubartsev, G. Manning, T. Nguyen, M. Olvera de la Cruz, A. Parsegian, R. Podgornik, D. Rau, and T. Thomas for discussions and correspondence.

Support from the Israel Science Foundation under grant No. 210/02, to B.S.F., is gratefully acknowledged. D.A. thanks the Alexander von Humboldt Foundation for a research award.

REFERENCES

Andelman, D. 1994. Electrostatic properties of membranes: the Poisson-Boltzmann theory. *In* Handbook of Physics of Biological Systems, Vol. I. R. Lipowsky, and E. Sackmann, editors. Elsevier Science, Amsterdam, pp.603–642.

Arenzon, J. J., J. F. Stilck, and Y. Levin. 1999. Simple model for attraction between like-charged polyions. *Eur. Phys. J. B.* 12:79–82.

Belloni, L., M. Drifford, and P. Turq. 1984. Counterion diffusion in polyelectrolyte solutions. *Chem. Phys.* 83:147–154.

Bloomfield, V. A., D. M. Crothers, and I. Tinoco. 2000. Nucleic Acids: Structures, Properties, and Functions. University Science Books, Sausalito, CA.

Borukhov, I., R. F. Bruinsma, W. M. Gelbart, and A. J. Liu. 2001. Elastically driven linker aggregation between two semiflexible polyelectrolytes. *Phys. Rev. Lett.* 86:2182–2185.

Borukhov, I., K.-C. Lee, R. F. Bruinsma, W. M. Gelbart, A. J. Liu, and M. Stevens. 2002. Association of two semiflexible polyelectrolytes by interchain linkers: theory and simulations. *J. Chem. Phys.* 117:462–480.

Braunlin, W. H., T. J. Strick, and M. T. Record, Jr. 1982. Equilibrium dialysis studies of polyamine binding to DNA. *Biopolymers.* 21:1301–1314.

Chattoraj, D. K., L. C. Gosule, and J. A. Schellman. 1978. DNA condensation with polyamines. II. Electron microscopic studies. *J. Mol. Biol.* 121:327–337.

Gelbart, W. M., R. F. Bruinsma, P. A. Pincus, and V. A. Parsegian. 2000. DNA-inspired electrostatics. *Phys. Today.* 53:38–44.

Gosule, L. C., and J. A. Schellman. 1978. DNA condensation with polyamines. I. Spectroscopic studies. *J. Mol. Biol.* 121:311–326.

Guéron, M., and G. Weisbuch. 1980. Polyelectrolyte theory. I. Counterion accumulation, site-binding, and the insensitivity to polyelectrolyte shape in solutions containing finite salt concentrations. *Biopolymers.* 19: 353–382.

Ha, B. Y., and A. J. Liu. 1997. Counterion-mediated attraction between two like-charged rods. *Phys. Rev. Lett.* 79:1289–1292.

Le Bret, M., and H. Zimm. 1984. Distribution of counterions around a cylindrical polyelectrolyte and Manning's condensation theory. *Biopolymers.* 23:287–312.

Lyubartsev, A. P., and L. Nordenskiöld. 1997. Monte Carlo simulation study of DNA polyelectrolyte properties in the presence of multivalent polyamine ions. *J. Phys. Chem. B.* 101:4335–4342.

Nguyen, T. T., I. Rouzina, and B. I. Shklovskii. 2000. Reentrant condensation of DNA induced by multivalent counterions. *J. Chem. Phys.* 112:2562–2568.

Nguyen, T. T., and B. I. Shklovskii. 2001. Complexation of DNA with positive spheres: phase diagram of charge inversion and reentrant condensation. *J. Chem. Phys.* 115:7298–7308.

Olvera de la Cruz, M., L. Belloni, M. Delsanti, J. P. Dalbiez, O. Spalla, and M. Drifford. 1995. Precipitation of highly charged polyelectrolyte solutions in the presence of multivalent salts. *J. Chem. Phys.* 103: 5781–5791.

Oosawa, F. 1971. Polyelectrolytes. Marcel Dekker, New York.

Osland, A., and K. Kleppe. 1977. Polyamine induced aggregation of DNA. *Nucleic Acids Res.* 4:685–695.

Pelta, J., D. Durand, J. Doucet, and F. Livolant. 1996a. DNA mesophases induced by spermidine: structural properties and biological implications. *Biophys. J.* 71:48–63.

Pelta, J., F. Livolant, and J.-L. Sikorav. 1996b. DNA aggregation induced by polyamines and cobalthexamine. *J. Biol. Chem.* 271:5656–5662.

Plum, G. E., and V. A. Bloomfield. 1988. Equilibrium dialysis study of binding of hexamine cobalt to DNA. *Biopolymers.* 27:1045–1051.

Raspaud, E., I. Chaperon, A. Leforestier, and F. Livolant. 1999. Spermine-induced aggregation of DNA, nucleosome and chromatin. *Biophys. J.* 77:1547–1555.

Raspaud, E., M. Olvera de la Cruz, J.-L. Sikorav, and F. Livolant.1998. Precipitation of DNA by polyamines: a polyelectrolyte behavior. *Biophys. J.* 74:381–393.

Rau, D. C., B. Lee, and V. A. Parsegian. 1984. Measurement of the repulsive force between poly-electrolyte molecules in ionic solution-hydration forces between parallel DNA double helices. *Proc. Natl. Acad. Sci. USA.* 81:2621–2625.

Rau, D. C., and V. A. Parsegian. 1992a. Direct measurement of the intermolecular forces between counterion-condensed DNA double helices. *Biophys. J.* 61:246–259.

Rau, D. C., and V. A. Parsegian. 1992b. Direct measurement of temperature-dependent solvation forces between DNA double helices. *Biophys. J.* 61:260–271.

Saminathan, M., T. Antony, A. Shirahata, L. H. Sigal, T. Thomas, and T. J. Thomas. 1999. Ionic and structural specificity effects of natural and synthetic polyamines on the aggregation and resolubilization of single-, double-, and triple-stranded DNA. *Biochemistry.* 38:3821–3830.

Strey, H. H., R. Podgornik, D. C. Rau, and V. A. Parsegian. 1998. DNA-DNA interactions. *Curr. Opin. Struct. Biol.* 8:309–313.

Subirana, J. A., and J. L. Vives. 1981. The precipitation of DNA by spermine. *Biopolymers.* 20:2281–2283.

Tabor, C. W., and H. Tabor. 1984. Polyamines. *Annu. Rev. Biochem.* 53:749–790.

Tang, J. X., T. Ito, T. Tau, P. Traub, and P. A. Janmey. 1997. Opposite effects of electrostatics and steric exclusion on bundle formation by F-actin and other filamentous polyelectrolytes. *Biochemistry.* 36:12600–12607.

Widom, J., and R. L. Baldwin. 1980. Cation-induced toroidal condensation of DNA. *J. Mol. Biol.* 144:431–453.

Widom, J., and R. L. Baldwin. 1983. Monomolecular condensation of λ-DNA induced by cobalt hexamine. *Biopolymers.* 22:1595–1620.

Wilson, R. W., and V. A. Bloomfield. 1979. Counterion-induced condensation of deoxyribonucleic acid. A light scattering study. *Biochemistry.* 79:2192–2196.

Wilson, R. W., D. C. Rau, and V. A. Bloomfield. 1980. Comparison of polyelectrolyte theories of the binding of cations to DNA. *Biophys. J.* 30:317–325.

Wittmer, J., A. Johner, and J. F. Joanny. 1995. Precipitation of polyelectrolytes in the presence of multivalent salts. *J. Phys. II France.* 5:635–654.